Marine and Petroleum Geology 82 (2017) 69–84

Contents lists available at ScienceDirect

Marine and Petroleum Geology

journal homepage: www.elsevier.com/locate/marpetgeo

Research paper

Identification of sedimentary-diagenetic facies and reservoir porosity and permeability prediction: An example from the Eocene beach-bar sandstone in the Dongying Depression, China

Jian Wang [a, b, *], Yingchang Cao [a, b, **], Keyu Liu [a, c], Jie Liu [d], Muhammad Kashif [a]

[a] School of Geosciences, China University of Petroleum (East China), Qingdao 266580, China
[b] Laboratory for Marine Mineral Resources, Qingdao National Laboratory for Marine Science and Technology, Qingdao 266071, China
[c] Department of Applied Geology, Curtin University, GPO Box U1987, Perth, WA 6845, Australia
[d] Post-doctoral Research Center of Geological Resources and Geological Engineering, China University of Petroleum (East China), Qingdao 266580, China

ARTICLE INFO

Article history:
Received 4 May 2016
Received in revised form
5 October 2016
Accepted 2 February 2017
Available online 4 February 2017

Keywords:
Reservoir prediction
Sedimentary-diagenetic facies
Log
Beach-bar sandstone
Dongying depression

ABSTRACT

Accurate prediction of reservoir porosity and permeability is essential for prospecting hydrocarbon reserves and petroleum production capacity. We propose an innovative reservoir porosity and permeability prediction method through identifying sedimentary-diagenetic facies, determining the porosity-permeability trends using core measurement data, extrapolating the spatial distribution of the sedimentary-diagenetic facies using log data through the Bayes discriminant analysis and predicting the reservoir porosity and permeability. The essence of the method was illustrated and its effectiveness was demonstrated using the Eocene beach-bar sandstones in the Dongying Depression, Bohai Bay Basin, eastern China. The Eocene beach bar sandstones are classified into fine sandstone, siltstone, and argillaceous siltstone based on grain sizes, sorting, and matrix contents. The major diagenetic processes that influence the porosity and permeability of the beach-bar sandstones are compaction, carbonate cementation and feldspar dissolution. Seven sedimentary-diagenetic facies were identified in the beach-bar sandstones based on the lithological types, and their corresponding diagenesis and influence extent on reservoir properties. The variation ranges of porosity and permeability (log K) of these sedimentary-diagenetic facies are typically less than 6% and 1.2, respectively. Both the porosity and permeability have well defined functional relationships with depth. The sedimentary-diagenetic facies can be identified effectively from logging data through the use of the Bayes discriminant analysis and corresponding cross-plots. The porosity and permeability (log K) of the well evaluated in the study were predicted with errors in the range of ±3% and ±0.6, respectively, based on the distribution and the fitting equation of the trend lines for the seven sedimentary-diagenetic facies. The predicted porosities and permeability of sedimentary-diagenetic facies match the measured porosities and permeability well.

1. Introduction

Reservoir porosity and permeability are critical parameters for petroleum exploration and production. Reservoir porosity determines the hydrocarbon storage capacity (reserves for a prospect), whereas permeability controls the hydrocarbon production capacity (Worden et al., 2000). The success of many hydrocarbon exploration efforts depends mainly on finding reservoirs with sufficient porosity and permeability to support viable commercial development (Taylor et al., 2010). Consideration of how the porosity and permeability vary within sand bodies, determination of reservoir petrophysical properties and the use of distribution models are all important for reservoir prediction (Bloch, 1991; Dutton and Diggs, 1992). The heterogeneous nature of sandstone may contribute to the considerable variabilities and wide distribution ranges of porosity and permeability (Bloch, 1991; Dutton and Diggs, 1992).

Many reservoir prediction models have been proposed, including spatial and temporal distribution models of sedimentary

* Corresponding author. School of Geosciences, China University of Petroleum, Qingdao, Shandong 266580, China.
** Corresponding author. School of Geosciences, China University of Petroleum (East China), Qingdao 266580, China.
E-mail addresses: wangjian8601@upc.edu.cn (J. Wang), caoych@upc.edu.cn (Y. Cao).

http://dx.doi.org/10.1016/j.marpetgeo.2017.02.004
0264-8172/

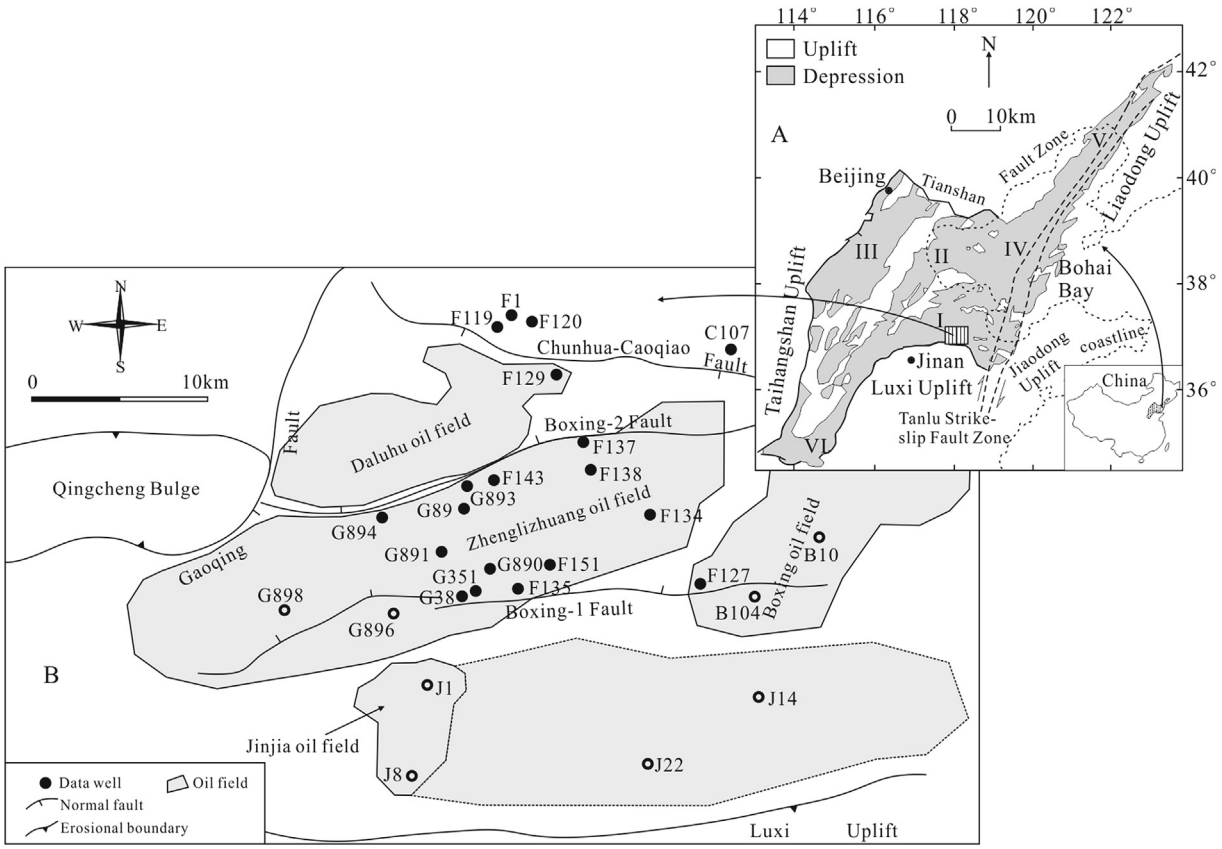

Fig. 1. (A) Tectonic setting of the Boxing sag in the Dongying Depression, southern Jiyang subbasin (I) of the Bohai Bay Basin. Other subbasins in the Bohai Bay Basin include the Huanghua subbasin (II), Jizhong subbasin (III), Linqing subbasin (IV), Bozhong subbasin (V) and Liaohe subbasin (VI). (B) Structural map of the Boxing sag with the well locations and the main faults in the Es4s unit.

facies and diagenetic facies within sequence stratigraphy frameworks (Morad et al., 2000; Taylor et al., 2000; Ketzer et al., 2003; Al-Ramadan et al., 2005), process-based models for early grain coats and their impact on deep reservoir quality (Ajdukiewicz et al., 2010), normal compaction, porosity-depth or porosity-temperature curve models (Schmoker and Schenk, 1994; Lander and Walderhaug, 1999; Ehrenberg et al., 2008; Ajdukiewicz and Lander, 2010; Taylor et al., 2010), burial history reconstruction models, and thermodynamic reservoir quality prediction models that include petrographic data describing the sediment texture, composition and early cement attributes (Schmoker and Gautier, 1988; Bjørkum et al., 1998; De Souza and McBride, 2000; Walderhaug, 2000; Bloch et al., 2002; Paxton et al., 2002; Ajdukiewicz and Lander, 2010; Taylor et al., 2010; Tobin et al., 2010). Most of these prediction models are intended to obtain porosity/permeability-depth or porosity/permeability-temperature trend lines with relatively narrow distribution ranges of porosity and permeability. However, most of the prediction models still have limitations because of other controlling factors that are not well constrained (Marchand et al., 2002; Ajdukiewicz and Lander, 2010).

The reservoir porosity and permeability of sandstones is largely controlled by sedimentary textures and diagenetic processes (Salem et al., 2005; McKinley et al., 2011). Sedimentary textures, including grain size, sorting, matrix content and clastic component content, are referred as lithofacies (Okoro and Igwe, 2014; Shinn et al., 2014). The final products of diagenetic processes are combinations of a series of diagenetic environments and diagenetic events, which are called diagenetic facies (Mou and Brenner, 1982; Liu et al., 2015). Diagenesis is usually related to the sedimentary facies (Rossi et al., 2001; Morad et al., 2010). The combination of lithofacies and corresponding diagenetic facies is defined as a sedimentary-diagenetic facies. Theoretically, sedimentary-diagenetic facies with the same depth range and formed in a specific depositional environment typically have similar characteristics of reservoir porosity and permeability. The reservoir porosity and permeability of uncored well sections may thus be predicted by the identification of sedimentary-diagenetic facies. Wireline logs are widely used to determine the lithology, sedimentary facies and diagenesis in areas where minimal core data are available (Selley, 1992; Ozkan et al., 2011).

This study focuses on the Eocene beach-bar sandstones in the Boxing sag of the Dongying Depression in the Bohai Bay Basin in East China (Fig. 1A and B). Here, a 200-m-thick succession of Eocene beach-bar sandstones and mudstones contains four economic low-permeability-tight oil fields at a depth of over 2300 m. Numerous studies have been performed on the beach-bar sandstone reservoirs over the past few years, but most of the research was focused on their sedimentary characteristics, depositional models, diagenesis and controlling factors of reservoir quality (e.g. Jiang et al., 2011; Guo et al., 2014). Research focusing on the prediction of high-quality reservoirs of the beach-bar sandstone is minimal, which impedes further exploration in the Dongying Depression. Therefore, prediction of high-quality reservoirs is crucial in developing effective exploration and development strategies for the study area.

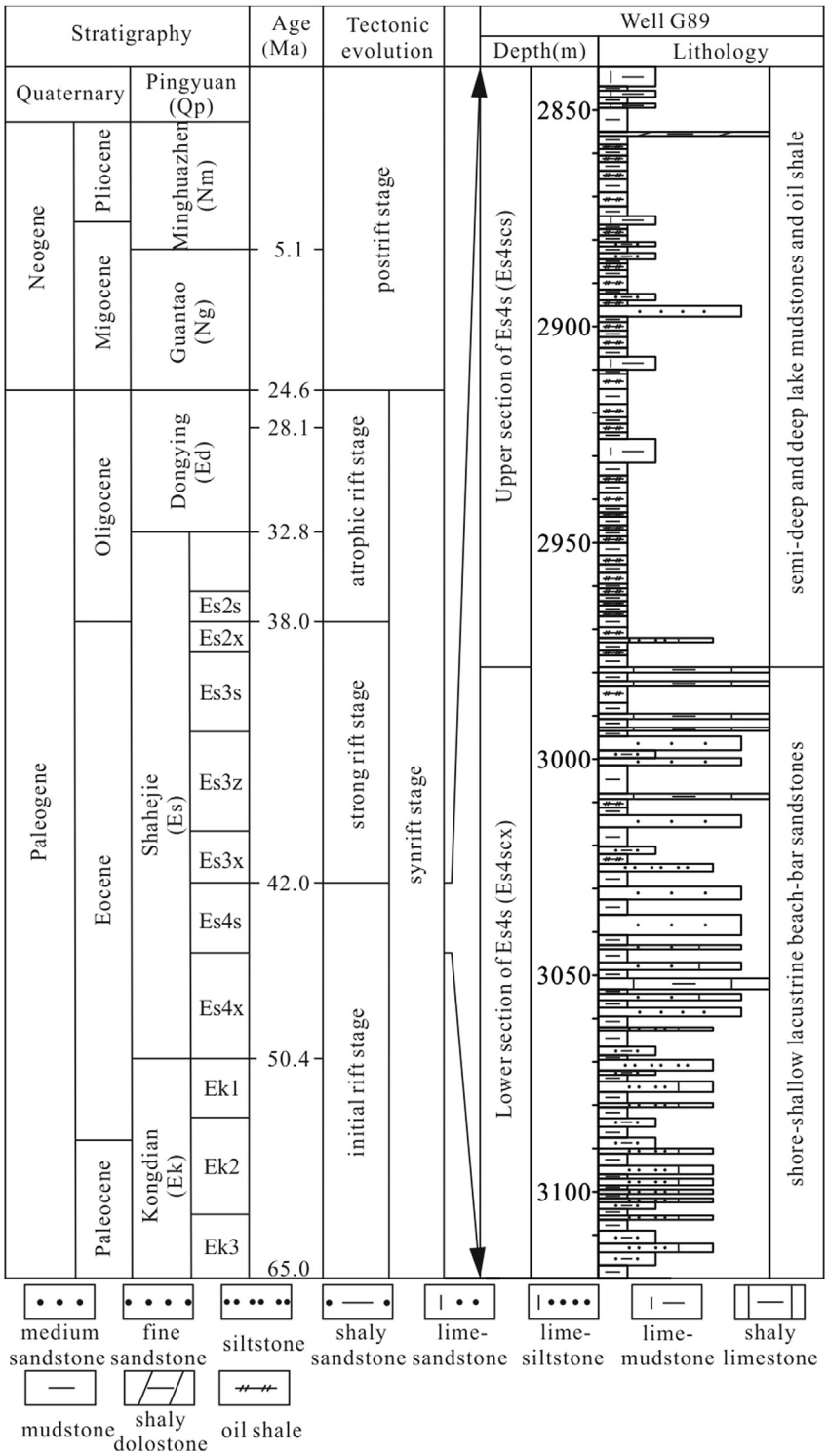

Fig. 2. Schematic Tertiary stratigraphy and tectonic evolution of the Boxing sag. The Es4s unit developed during the initial rift stage comprises sandstones that are interbedded with mudstones. Beach-bar sandstones mainly occur in the lower part of the Es4s formation.

To help fill these research gaps, we attempted to develop a new reservoir porosity and permeability prediction method based on a detailed study of the Boxing Sag, which is characterized by the typical beach-bar deposition during the Eocene (Jiang et al., 2011). In this study, we determined the sedimentary-diagenetic facies based on cores, thin sections and corresponding analytical measurements.

2. Geological setting

The Bohai Bay Basin, which is an important hydrocarbon-producing basin, is located on the eastern coast of China. The

Table 1
Grain compositions and characteristics of beach-bar sandstones in the study area.

Grain grade	Min	Max	Ave
Coarse sand (%)	0	9	2.7
Medium sand (%)	0	14.5	5.2
Fine sand (%)	9.4	88.8	53.2
Silty sand (%)	3.4	69.2	30
Mud (%)	0.4	23.5	8.9
Medium grain size (μm)	10	990	110
Sorting coefficient	1.28	4.63	1.76

basin is a complex rifted basin formed in the Late Jurassic through the Early Tertiary on the basement of the North China Platform. The tectonic evolution of the basin consists of a synrift stage (65.0–24.6 Ma) and a postrift stage (24.6 Ma to the present) (Lampe et al., 2012). The Boxing sag is a secondary tectonic unit of the Dongying Depression in the Bohai Bay Basin (Fig. 1A) comprising the Gaoqing fault in the west, Shicun fault in the east, Chunhua-Caoqiao fault in the north and Luxi Uplift in the south. The Boxing-1 and Boxing-2 faults are two second-order faults in the centre of the Boxing sag (Jiang et al., 2011). The Boxing sag is developed on a northward-dipping, subsiding faulted block within the Dongying Depression (Fig. 1B). The sag is filled with Cenozoic sediments including the Kongdian (Ek), Shahejie (Es), Dongying (Ed), Guantao (Ng), Minghuazhen (Nm) and Pingyuan (Qp) formations. The Es formation can be divided into four members from the base to the top, which are Es4, Es3, Es2 and Es1 (Fig. 2). The upper part of the Es4 member (Es4s) consists of fine-grained and thin-bedded sandstone interbedded with gray mudstone and is the focus of this study. The Es4s member was developed towards the end of the initial rift stage, which can be divided into the lower part (Es4scx) and the upper part (Es4scs). During the deposition of the Es4scx, large-scale near shore-shallow beach-bar sand bodies were developed under conditions of a gentle paleotopography, a shore-shallow lacustrine environment and a relatively abundant sediment supply. Large-scale dark gray mudstones and shale were developed during the deposition of the Es4scs and are the major hydrocarbon source rocks in the Boxing sag (Guo et al., 2014).

3. Samples and methods

Thirteen exploration wells were sampled for the investigation of the beach-bar sandstones (Fig. 1B). The sandstone core samples were impregnated with blue resin before petrographic thin sections were made to highlight pores. Carbonate minerals were stained with Alizarin Red S and Potassium ferricyanide for easy identification. Point-counting was carried out on 115 thin sections,

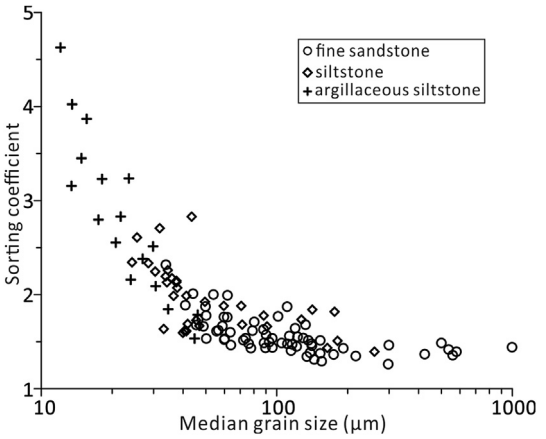

Fig. 4. Relationship between grain size and sorting coefficient of the Eocene beach-bar in the Boxing Sag.

Table 2
The compositions of the Eocene beach-bar sandstones in the Boxing Sag.

	Min	Max	Mean
Detrital grains			
Quartz (vol. %)	24.1	53.5	40.2
Potassium feldspars (vol. %)	8.4	25.6	16.8
Plagioclase feldspars (vol. %)	8.8	30.2	16.9
Volcanic lithic fragments (vol. %)	1.3	45.7	14
Metamorphic lithic fragments (vol. %)	5.1	19.6	10
Sedimentary lithic fragments (vol. %)	0	16.7	2.2
Mica (vol. %)	0	2.5	0.1
Chert (vol. %)	0	2.3	0.2
Matrix (vol. %)	0	27.6	9.9
Diagenetic alterations			
Calcite (vol. %)	0.5	30.2	6.5
Dolomite (vol. %)	0	17.4	2
Ankerite (vol. %)	0	2.3	0.95
Quartz overgrowths (vol. %)	0	3.5	0.2
Clay minerals (vol. %)	0	15	2.7
Kaolinite (%)	1	38	23.3
Illite (%)	25	71	43
Illite-smectite mixed layers (%)	3	53	26.7
Chlorite (%)	1	20	7
Pyrite (vol. %)	0	5.6	0.25
Porosity			
Intergranular porosity (vol. %)	0	17.2	2.8
Intragranular porosity (vol. %)	0	2.8	0.3

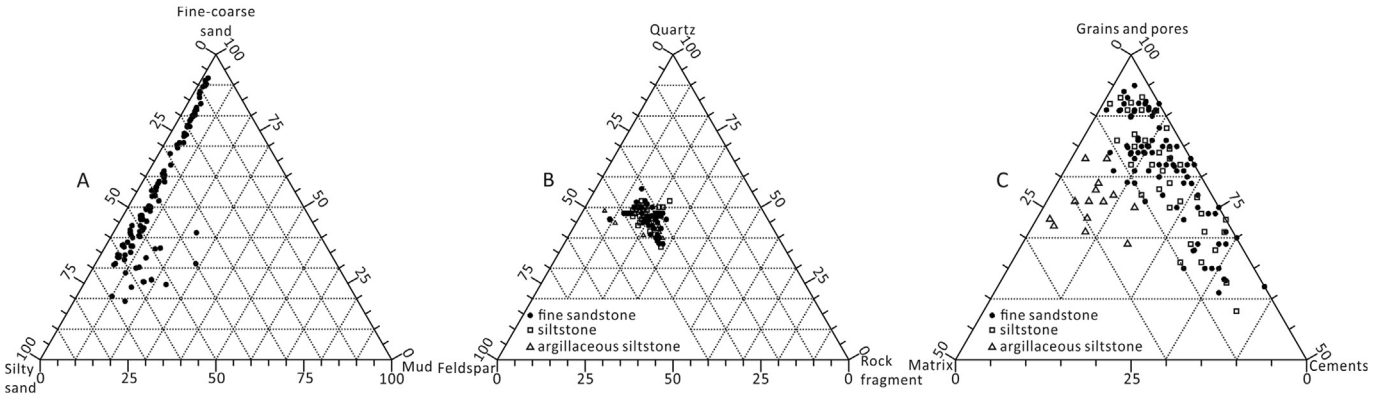

Fig. 3. The compositions of beach-bar sandstones of the Eocene beach-bar in the Boxing Sag.

Table 3
Characteristics of the lithofacies of fine sandstone, siltstone and argillaceous siltstone.

Rock types	Average grain size (μm)		Sorting coefficient		Matrix content (%)		Porosity (%)		Permeability (mD)	
	range	average	range	average	range	average	range	average	range	average
Fine sandstone	60–234	155	1.28–2.35	1.51	3–10	6.7	2.5–25	17.1	0.006–767	47.5
Siltstone	21–120	76	1.41–2.78	1.78	3–13	7.4	1.7–18.9	11.2	0.002–10.6	1.76
Argillaceous siltstone	10–94	63	1.52–4.63	2.79	8–22	15.6	2.2–15.2	6.8	0.007–7.2	0.13

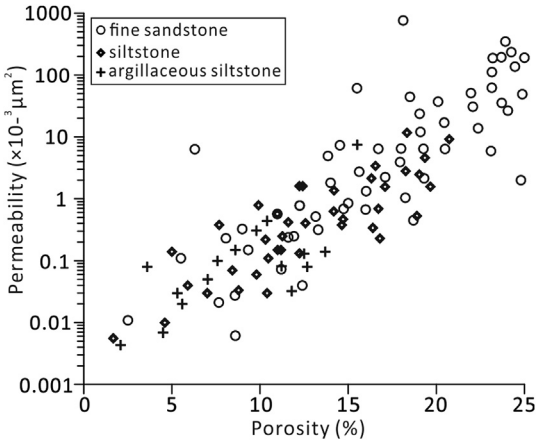

Fig. 5. Cross plot of porosity and permeability of the Eocene beach-bar sandstones in the Boxing Sag.

each of which were examined for 300 fields of view. Grain size analysis was conducted on photomicrographs using the AxioVisionRel.4.8 image analysis software with correction following the methods from Friedman (1958, 1962). The content of components with grain size less than 3.9 μm (matrix) were from visual estimation through microscope. The Udden-Wentworth grain size scale (Udden, 1914; Wentworth, 1922) was used and sorting ranking was determined in accordance with the standard charts of Folk (1974).

Clay minerals were analysed using the X-ray diffraction (XRD) method on a D8 DISCOVER with Cu-Ka radiation with a voltage of 40 kV, and a current of 25 mA. Before analysis, samples were oven-dried at 40 °C for 2 days. They were then ground in an agate mortar to less than 40 μm without using chemical pre-treatment. The samples were scanned from 3° to 70° with a step size of 0.02°. The relative content of the multiple mineral phases in weight percent was identified through diffractograms and semi-quantitatively analyses.

One inch diameter standard cylindrical core plugs were used to measured porosity and permeability. The porosity was measured following Boyle's Law on the basis of helium porosimeter measurements. The pre-processed samples (dry, clean) were injected with helium at approximately 200 psi in a porosimeter. The grain volume was calculated through the Boyle's Law equation by measuring the corresponding pressure and volume. The bulk volume of the sample was measured using the Archimedes Principle with mercury immersion and was used to determine the pore volume by subtracting the grain volume. The grain volume and bulk volume were then used to calculate the total porosity.

The logging data are derived from the in-house database of the Research Institute of Exploration and Development of the SINOPEC Shengli Oilfield. The Bayes discriminant analysis in this study was performed using the Statistical Product and Service Solutions (SPSS) software.

4. Results and interpretation

4.1. Sandstone compositions, types and effects on reservoir porosity and permeability

The grain sizes of the beach-bar sandstones investigated range from mud-size (less than 39 μm) to coarse-grained sand (1000 μm). The content of coarse-grained sand (500 μm-2000 μm), medium-grained sand (250 μm-500 μm), fine-grained sand (62.5 μm-250 μm), silt-size sand (3.9 μm-62.5 μm) and mud-size component (<3.9 μm) are summarized in Table 1. The grain sizes of the beach-bar sandstones are mainly fine-grained and silt-size sands. The coarse- and medium-grained sands are not considered separately but were summed together with fine-grained sands due to their low content. According to the grain size compositions, the beach-bar sandstones are classified into fine sandstones, siltstones and argillaceous siltstones (Fig. 3A). The sorting ranges from well (1.28) to poorly sorted (4.63). The sorting has positive relationships with the medium grain size of the fine sandstones, siltstone and argillaceous siltstone (Fig. 4).

The compositions of beach-bar sandstones are summarized in Table 2. The detrital compositions of fine sandstone, siltstone and argillaceous siltstone are mainly lithic arkoses according to Folk (1980) classification scheme, with corresponding average compositions for the three lithofacies being $Q_{44.9}F_{34.8}R_{20.3}$, $Q_{45.5}F_{34.4}R_{20.1}$, and $Q_{44.5}F_{35.7}R_{19.8}$ (Fig. 3B). There is no obvious difference in the clastic components between different lithofacies (fine sandstone, siltstone and argillaceous siltstone) with detrital quartz being the highest component. Detrital feldspars comprise both K-feldspar and plagioclase. Lithic fragments are mainly of volcanic and metamorphic types, with a small amounts of sedimentary in origin. Other detrital components include mainly small amounts of mica and chert (Table 2). The interstitial materials of the beach-bar sandstones consist mainly of argillaceous matrix and cements. The cements are dominated by carbonates including calcite, dolomite and ankerite with a minor amount of quartz overgrowths and clay minerals (Table 2). Pores in the beach-bar sandstones are dominated by intergranular pores (Table 2). According to the compositions the beach-bar sandstones are mainly classified into pure sandstones, calcareous sandstones and greywacke (Fig. 3B). Comprehensive analysis of grain sizes and lithological compositions of the beach-bar sandstones indicates that fine sandstones and siltstones are characterized by pure sandstones and calcareous sandstones, whereas argillaceous siltstones are dominated by greywacke (Fig. 3C). The characteristics and reservoir petrophysical properties of fine sandstone, siltstone and argillaceous siltstone are shown in Table 3.

The porosity and permeability of the fine sandstone, siltstone and argillaceous siltstone spread over wide ranges with the fine sandstone having the widest porosity and permeability distribution (Table 3 and Fig. 5). The minimum porosity and permeability of the three lithofacies are in the same range, while the maximum porosity and permeability of the fine sandstone is much higher than that of siltstone and argillaceous siltstone (Table 3 and Fig. 5).

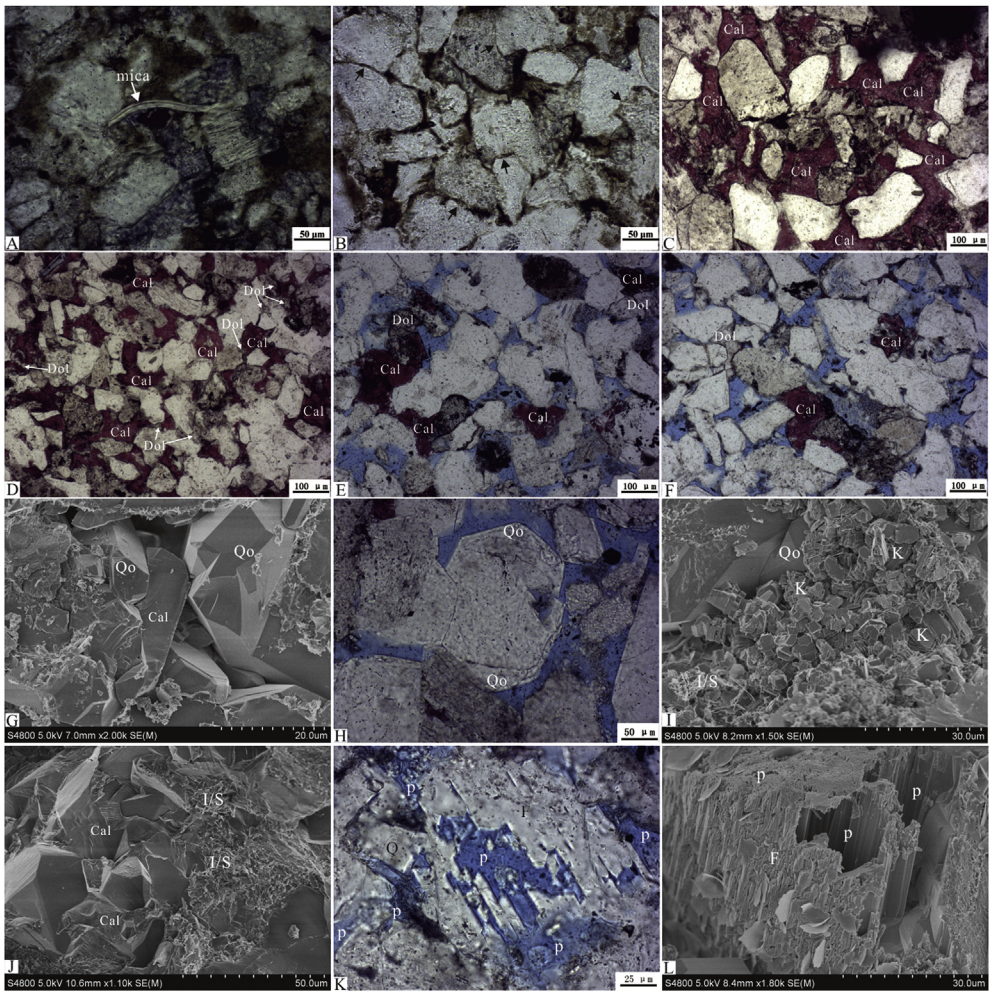

Fig. 6. Photomicrographs from optical and scanning electron microscopy showing the main types of diagenesis occurred in the Eocene beach-bar sandstones in the Dongying Depression. (A) Deformation of micas from Well F-137 at 3169.7 m (-). (B) Line-concavo-convex contact between grains from Well F-1 at 3308.61 m (-). (C) Crystalline carbonate cements in the boundary of sandstone from Well G-351 at 2464.79 m (-); (D) Coarse-crystalline calcites and minor amounts of dolomites filling in intergranular pores in the boundary of sandstone from Well G-351, 2455.14 m (-). (E) Coarse crystalline calcites and dolomites filling in intergranular pores in the centre of sandstone from Well G-890, 2598.2 m (-). (F) Coarse crystalline calcites and dolomites filling in intergranular pores in the centre of sandstone from Well G-890, 2598.2 m (-). (G) Quartz overgrowths and calcite from Well F-151-1 at 2685.5 m. (H) Quartz overgrowths from Well G-890 at 2598.2 m. (I) Quartz overgrowths, kaolinite and mixed-layer illite/smectite filling in pores from Well G-890 at 2599.2 m. (J) Carbonate cement and mixed-layer illite/smectite filling in pores from Well G-351 at 2464.79 m. (K) Dissolution pores in feldspar grains from Well G-890 at 2599.7 m (-). (L) Dissolution pores in feldspar grains from Well F-151-1 at 2701 m. P-pore, Q-quartz, F-feldspar, Cal-calcite, Dol-dolomite, Qo-quartz overgrowth, K-kaolinite, I/S-illite-smectite mixed layers, P-pores, (-) indicates the plane polarized light.

The porosity and permeability have positive relationships with grain size and sorting and have negative relationships with matrix contents (Table 3). The porosity and permeability of the three lithofacies all show good positive linear relationships (Fig. 5).

4.2. Diagenesis and effects on reservoir porosity and permeability

4.2.1. Compaction

Evidence of compaction in the beach-bar sandstones is abundant petrographically, including line contacts, line-concavo-convex contacts and deformed ductile grains (e.g., mica) (Fig. 6A and B). The initial intergranular volume (initial porosity) of the beach-bar sandstones in the study area is between 25.9% and 38.8%, with an average of 34.6% as calculated using Beard and Weyl's method (1973).

$$P_{primary} = 20.91 + (22.9/S_o) \quad (1)$$

$P_{primary}$, primary porosity; S_o, sorting coefficient.

The pore volume destroyed by compaction ($V_{compaction}$) is calculated using Equation (2) and the porosity compaction loss percentage ($P_{compaction}$) is calculated using Equation (3).

$$V_{compaction} = V_{primary} + V_{dissolution} - V_{cementation} - V_{present} \quad (2)$$

$$P_{compaction} = (V_{compaction}/V_{primary}) \times 100\% \quad (3)$$

$V_{primary}$, primary pore volume; $V_{compaction}$, pore volume destroyed by compaction; $V_{dissolution}$, dissolution pore volume; $V_{present}$, present pore volume; $P_{compaction}$, porosity compaction loss percentage.

The pore volumes that are destroyed by compaction are estimated to be 0.8%–24.4% (av. 12.1%), 0.5%–27.3% (av. 15.2%), and

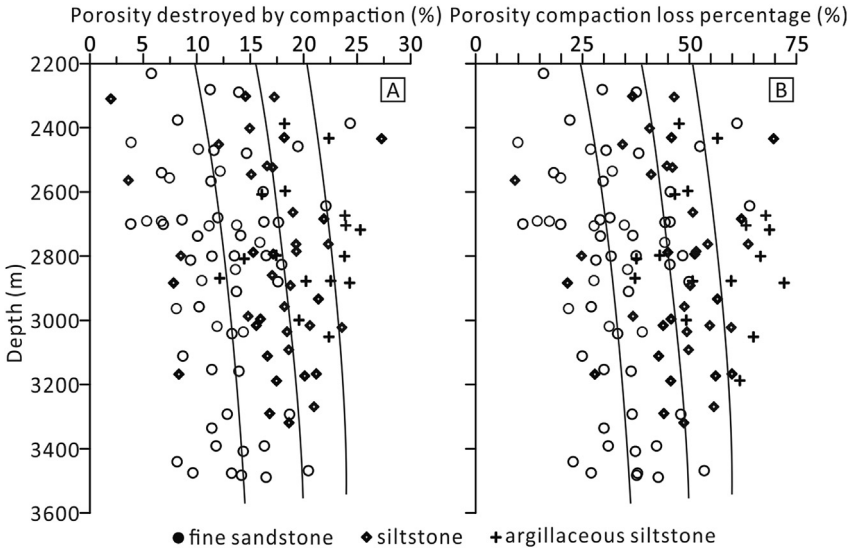

Fig. 7. Depth plots of pore volume destroyed by compaction and the porosity compaction loss percentage of the Eocene beach-bar sandstones in the Boxing Sag.

12.2%–26.5% (av. 20.2%), respectively, for fine sandstones, siltstones and argillaceous siltstones with corresponding porosity compaction loss rates being 2.1%–61.1% (av. 33.1%), 1.5%–69.7% (av. 41.5%), and 37.3%–70.8% (av. 55%). The V $_{compaction}$ and the $P_{compaction}$ of fine sandstones, siltstones and argillaceous siltstones have an increasing trend with burial depths (Fig. 7). At the same burial depth the V $_{compaction}$ and the $P_{compaction}$ of the fine sandstones are the lowest, while the V $_{compaction}$ and the $P_{compaction}$ of the argillaceous siltstones are the highest, and that of the siltstones is in-between (Fig. 7).

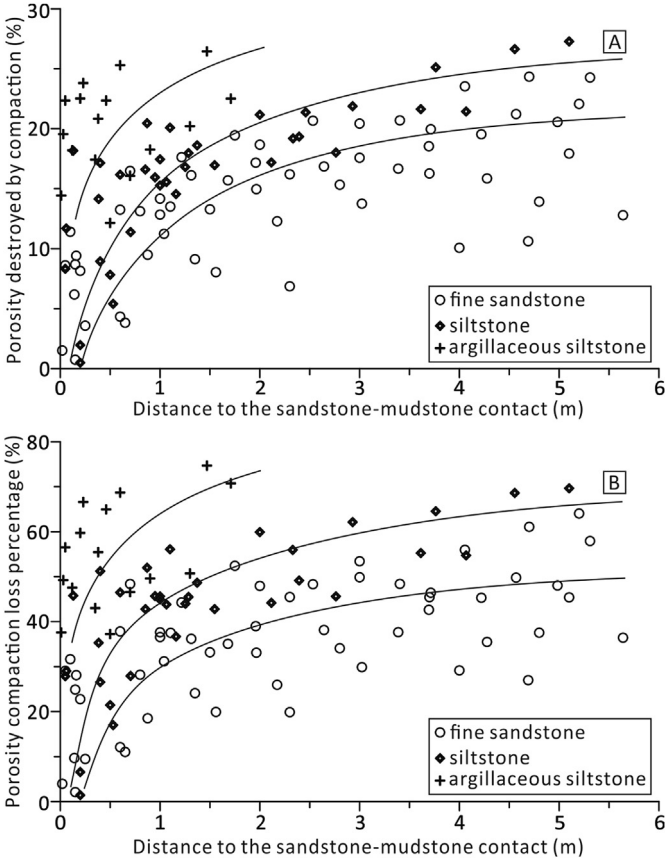

Fig. 8. Cross plots between (A) pore volume destroyed by compaction and (B) the porosity compaction loss percentage and the distance to the mudstone-sandstone contacts of the Eocene beach-bar sandstones in the Boxing Sag.

The V $_{compaction}$ and $P_{compaction}$ of fine sandstones, siltstones and argillaceous siltstones apparently increase from the mudstone-sandstone contact to the centre of sandstones (Fig. 8). The compaction for argillaceous siltstones is stronger than that for the siltstones and fine sandstones because of the fine grain size, poor sorting and high matrix content. For the siltstones and fine sandstones, the V $_{compaction}$ and $P_{compaction}$ increase sharply in the vicinity of the boundaries of sandstones (less than 1 m to the contact), while the V $_{compaction}$ and the $P_{compaction}$ increase gently in the centre of sandstones (1 m further away from the contact). Therefore, compaction has different impacts on different types of lithofaciess and on different parts of the same lithofacies. The contact styles of grains also indicate the different impacts of compaction. The grains mainly show non-contact and point contacts near the boundaries of sandstones (Fig. 6C and D), while the grains mainly show point-line and line contacts in the centre of sandstones (Fig. 6E and F).

4.2.2. Cementation

The cement types in the beach-bar sandstone reservoirs in the Boxing sag consist mainly of carbonates, authigenic quartz and clay minerals (Fig. 6). Carbonate cement has the highest content (Table 2) and mainly fills primary intergranular pores and dissolution pores. The influence on reservoir porosity and permeability of the carbonate cements that fill the pores is much bigger than that of the cement that surrounds grains (e.g., quartz overgrowths) (Fig. 6G, H, I; Carvalho et al., 1995; Dutton, 2008; Morad et al., 2010). The volumes of carbonate cements and authigenic quartz in the beach-bar sandstones are 0.3%–28% (av. 9.7%) and 0–3.5% (av. 0.2%), respectively. Authigenic quartz is usually formed as partial or whole overgrowth rims around quartz grains (Fig. 6G, H, I). The clay in the beach-bar sandstones mainly includes clay matrix and authigenic clay minerals that formed during diagenetic processes. The XRD results indicates that the content of clay in the beach-bar sandstones is mainly between 0 and 19.6%, with an average of 9.1 wt %. Although the clay minerals generally experienced transformation from smectite and kaolinite to illite or chlorite during the

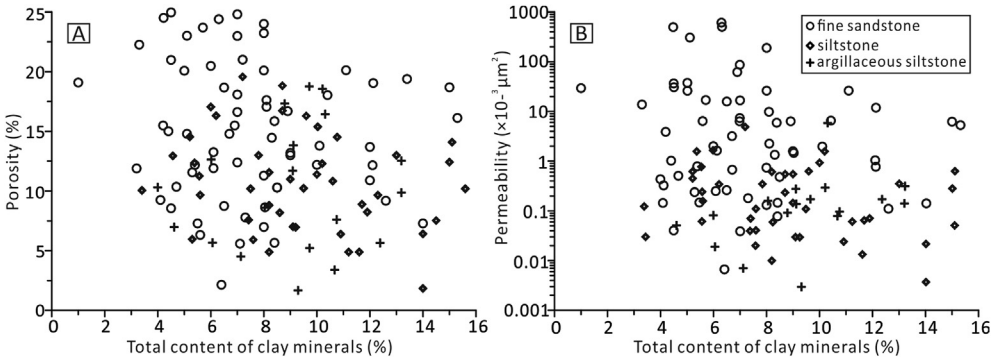

Fig. 9. Crossplots of the total clay minerals content and the porosity and permeability of the Eocene beach-bar sandstones in the Boxing sag.

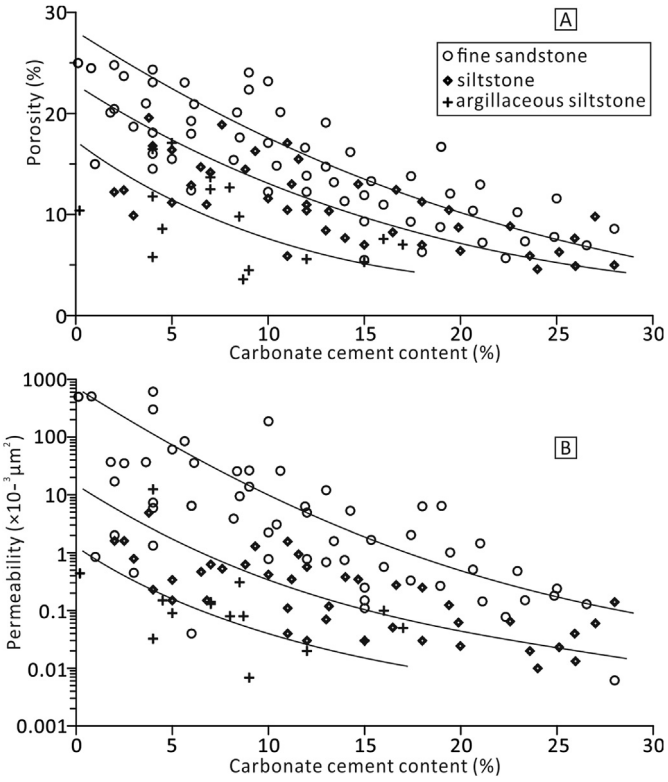

Fig. 10. Cross plots of the carbonate cement content and the porosity and permeability of the Eocene beach-bar sandstones in the Boxing sag.

burial process, the volume of authigenic clay minerals filling in the intergranular pores is very small (less than 5 vol %) from microscopic and SEM observation and point counting. Most of the clay minerals in the beach-bar sandstones are corresponding to the clay matrix and occur as laminations (Fig. 6I and J). The relationships between the content of total clay minerals and porosity and permeability in fine sandstone, siltstone and argillaceous siltstone indicate that the influences on reservoir property from the total clay minerals of the beach-bar sandstones are quite limited (Fig. 9). Compared with quartz overgrowth and authigenic clay minerals, the effect of the carbonate cements on reservoir quality is very strong. The carbonate cement shows a strong negative correlation with the porosity and permeability of the fine sandstone, siltstone and argillaceous siltstone (Fig. 10). Samples with high porosity and permeability usually have low contents of carbonate cement. Therefore, the distribution of carbonate cements controls the reservoir property greatly.

All samples in this study have certain amounts of carbonate cements, with an extremely heterogeneous distribution in the reservoirs. Only the samples along the sandstone-mudstone contact have high carbonate cement contents, and these sandstones exhibit tightly cemented features (Fig. 6C, D, E, and F). For instance, the carbonate cement contents from 3165 m to 3174 m in the sandstones near the sandstone-mudstone contact in Well F-137 is high (average 20.2%), while the carbonate cement contents in the middle of the sandstone is relatively low (average 9.6%) (Fig. 11). The porosity and permeability at the edge of the sandstone is very low (average 6.3% and 0.076 $\times$ 10^{-3} μm^2, respectively). However, the porosity and permeability in the middle of the sandstone is high (average 11.8% and 0.68 $\times$ 10^{-3} μm^2, respectively).

The sources of the carbonate cements in clastic reservoirs are external and internal (Dutton, 2008). The amount of carbonate rock fragments in the beach-bar sandstone is very low and insufficient to serve as the source for the carbonate cements. Due to the aforementioned distribution characteristics, the carbonate cements in the beach-bar sandstones are external and are most likely related to the diagenesis of the interbeded mudstones (Milliken and Land, 1993; Li et al., 2014). The sources of the carbonate cements are predominantly from bioclasts (Carvalho et al., 1995), the dissolution of detrital carbonate rock fragments (Carvalho et al., 1995; Dutton, 2008), the conversion of smectite to illite (Boles and Franks, 1979; McHargue and Price, 1982; Li et al., 2014), K-feldspar dissolution and the corresponding conversion of kaolinite to illite in the mudstones (Macaulay et al., 1993; Li et al., 2014). A chemical gradient can be produced from the unbalanced distributions of reactive components between adjacent sandstones and mudstone, which may have caused the mass transfer between lithological units via diffusion (Chen et al., 2009; Li et al., 2014; Wang et al., 2016). During this transportation from mudstone to sandstone, the initial chemical balance is broken by water-rock reactions in the new chemical environment, allowing carbonate cements to form along the edges of the sandstones (Milliken and Land, 1993; Dutton, 2008; Chen et al., 2009; Li et al., 2014; Wang et al., 2016). Therefore the different distributions of carbonate cements influenced the destruction of the porosity through cementation in different positions of sandstones (Fig. 12). The pore volume destroyed by cementation ($V_{cementation}$) is equal to the volume of carbonate cements and the porosity cementation loss percentage ($P_{cementation}$) is calculated using Equation (4).

$$P_{cementation} = (V_{cementation}/V_{primary}) \times 100\% \quad (4)$$

$P_{cementation}$, porosity cementation loss percentage.

For the fine sandstones, siltstones and argillaceous siltstones,

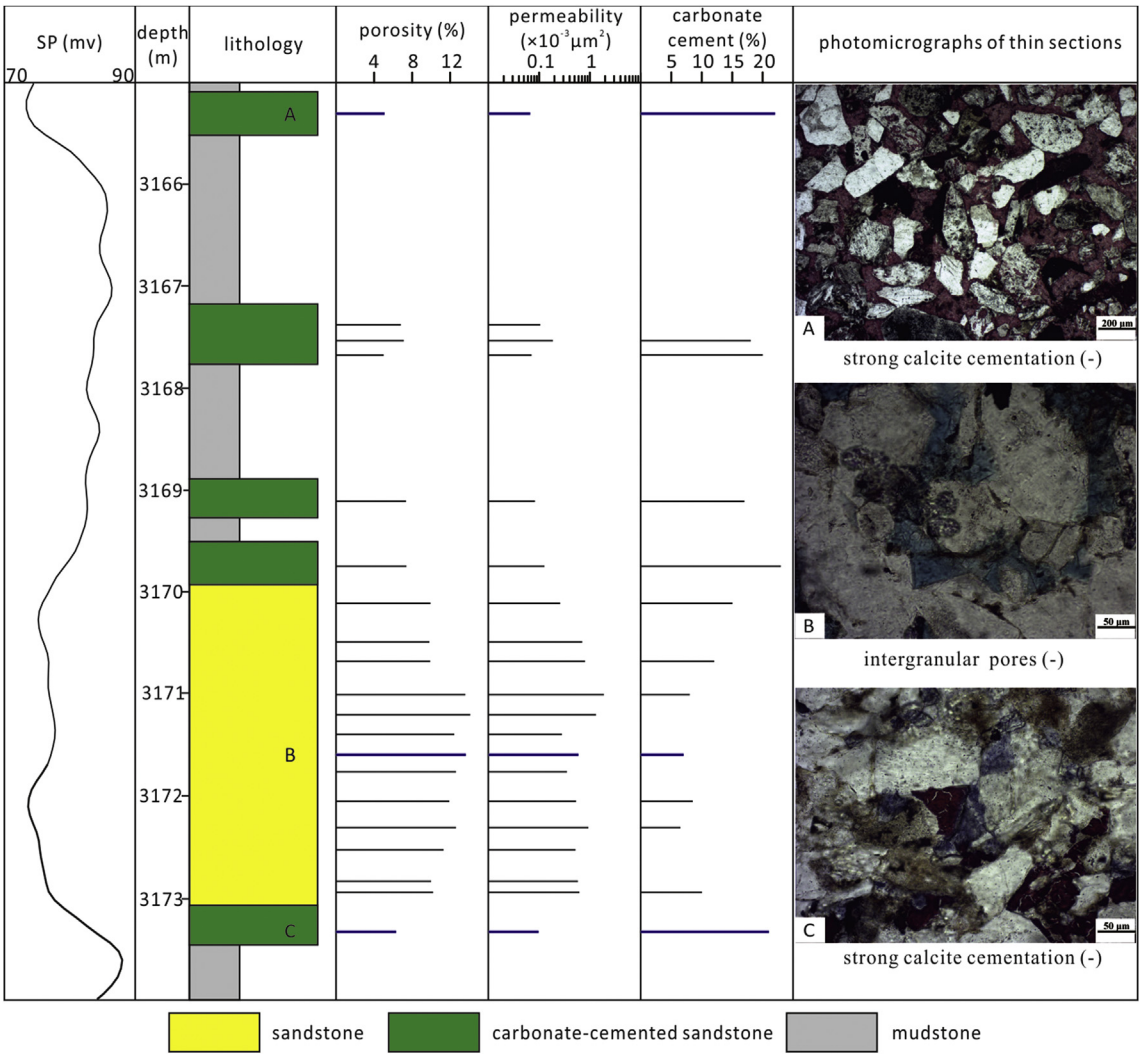

Fig. 11. Stratigraphy and reservoir quality of Well F-143. Note the strong heterogeneity associated with carbonate cementation along the sandstone-mudstone contacts. Thin beach-bar deposits are prone to becoming completely cemented by carbonate.

the pore volumes that are destroyed by carbonate cementation are 0.3%–28% (av. 9.2%), 2.6%–27% (av. 11.2%), and 0.3%–17% (av. 8.4%), respectively, whereas the porosity cementation loss rates are 0.9%–52.6% (av. 25.7%), 6.6%–80.6% (av. 31.6%), and 0.9%–44.3% (av. 22.3%), respectively. This indicates that the carbonate cementation is also an important factor in controlling the porosity reduction in the beach-bar sandstones. The $V_{cementation}$ and $P_{cementation}$ of fine sandstones, siltstones and argillaceous siltstones decrease apparently from the boundaries to the centres of sandstones (Fig. 12). The $V_{cementation}$ and $P_{cementation}$ of the argillaceous siltstones are lower than that of the fine sandstones and siltstones. When the distance to the sandstone-mudstone contact is less than 1 m, the $V_{cementation}$ and $P_{cementation}$ of the fine sandstones and siltstones are usually high and decrease rapidly away from the contacts. When the distances to the sandstone-mudstone contacts are more than 1 m, the $V_{cementation}$ and $P_{cementation}$ of the fine sandstones and siltstones are low and decreases slowly with increasing distances to the contacts. Early strong carbonate cementation is known to prevent compaction (Budd, 2002; Morad et al., 2010), but the compaction-resistance capacity in the middle thick sandstones, which have low carbonate cement content, is relatively weak. Hence, the $V_{compaction}$ and $P_{compaction}$ at the boundaries of sandstones are lower than that in the centres of the sandstones. The tight carbonate cementation causes the calcareous fine sandstones and calcareous siltstones are mainly distributed at the boundary of sandstones and siltstones.

4.2.3. Dissolution

Dissolution in the beach-bar sandstones mainly occurred in feldspars (Fig. 6K and L). The volumes of dissolution pores in the fine sandstone, siltstone and argillaceous siltstone are 0–5.8% (av. 2.1%), 0–3.5% (av. 1.5%), and 0–2.7% (av. 0.8%), respectively, from the point-counting. The correlations between the dissolution porosity and porosity and permeability of the fine sandstone, siltstone and argillaceous siltstone indicate that dissolution improves the reservoir porosity to some extent (Fig. 13A) but have no apparent influence on reservoir permeability (Fig. 13B). The pore volume increased by dissolution ($V_{dissolution}$) is equal to the volume of dissolution pores, and the porosity dissolution increment percentage ($P_{dissolution}$) is calculated using Equation (5).

$$P_{dissolution} = (V_{dissolution}/V_{present}) \times 100\% \quad (5)$$

$P_{dissolution}$, porosity dissolution increment percentage.

Affected by the tight carbonate cementation at the boundaries

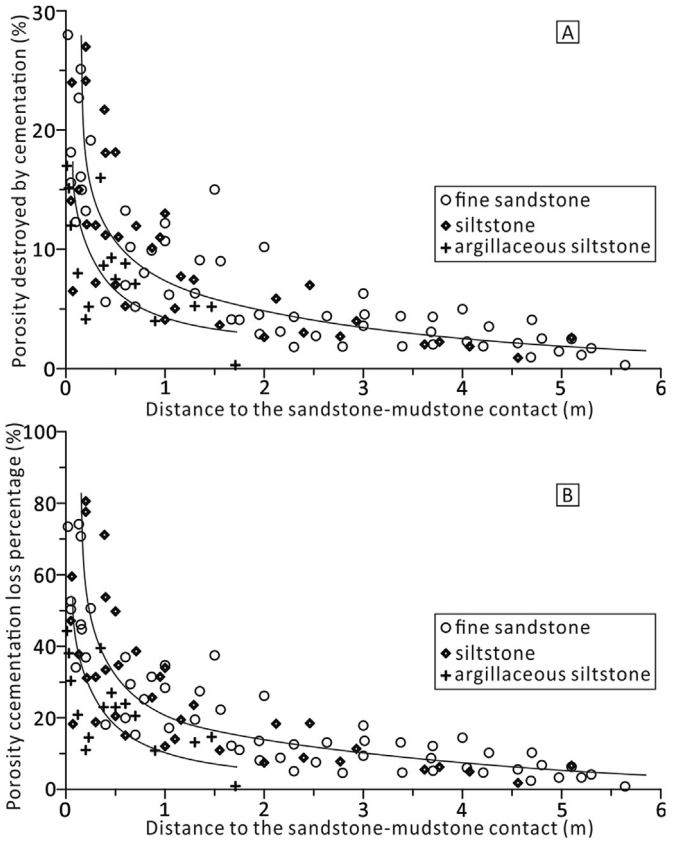

Fig. 12. Cross plots between (A) pore volume destroyed by cementation and (B) the porosity cementation loss percentage and distance to the mudstone-sandstone contacts of the Eocene beach-bar sandstones in the Boxing Sag.

of sandstones, the fluids causing the dissolution mainly distribute in the centres of the thick beach-bar sandstones, which makes the dissolution pore volumes correlate positively with the distances to the sandstone-mudstone contacts in the fine sandstone, siltstone and argillaceous siltstone (Fig. 14A). The $P_{\text{dissolution}}$ of samples in the centres of sandstones (more than 1 m to the sandstone-mudstone contact) has a positive relationship with the distances to the sandstone-mudstone contacts. The $P_{\text{dissolution}}$ of samples (ranging between 0 and 40%) near the boundaries of sandstones (within 1 m to the sandstone-mudstone contacts) has no apparent relationship with the distances to the sandstone-mudstone contacts (Fig. 14B). Tight carbonate cementation destroyed most of the intergranular pores near the boundary of the sandstones. Although the $P_{\text{dissolution}}$ of some samples located at the edge of sandstones is high, the dissolution pore volume of these samples is very low (Fig. 14B).

5. Discussion

5.1. Types and petrophysical properties of sedimentary-diagenetic facies

The diagenetic events and the extent of their impact on the petrophysical properties of a reservoir are the main factors in considering the classification of diagenetic facies in clastic reservoirs (Liu et al., 2015; Mou and Brenner, 1982). Compaction mainly affects the reservoir quality in the centre of the fine sandstone and siltstone and in the argillaceous siltstone. The influence extent of compaction on the reservoir quality is quite minor at the boundaries of the fine sandstone and siltstone. Cementation mainly affects the reservoir quality of the boundaries of fine sandstone, siltstone and argillaceous siltstone. The influence extent of cementation on reservoir quality is very small in the centre of the fine sandstone and siltstone. Dissolution also mainly affects the reservoir quality in the centre of the fine sandstone and siltstone. The classification standard for the influence extent on the reservoir quality of compaction, carbonate cementation and dissolution are summarized in Table 4.

Seven sedimentary-diagenetic facies are classified based on Table 4 and the analysis of diagenesis in the fine sandstone, siltstone and argillaceous siltstone. They include: (1) medium compaction-weak feldspar dissolution-weakly carbonate cemented siltstone facies (Type A), (2) medium compaction-weak feldspar dissolution-moderately carbonate cemented fine sandstone facies (Type B), (3) medium compaction-weak feldspar dissolution-weakly carbonate cemented siltstone facies (Type C), (4) medium compaction-weak feldspar dissolution-moderately carbonate cemented siltstone facies (Type D), (5) weak compaction-weak feldspar dissolution-strongly carbonate cemented fine sandstone facies (Type E), (6) weak compaction-weak feldspar dissolution-strongly carbonate cemented siltstone facies (Type F), and (7)

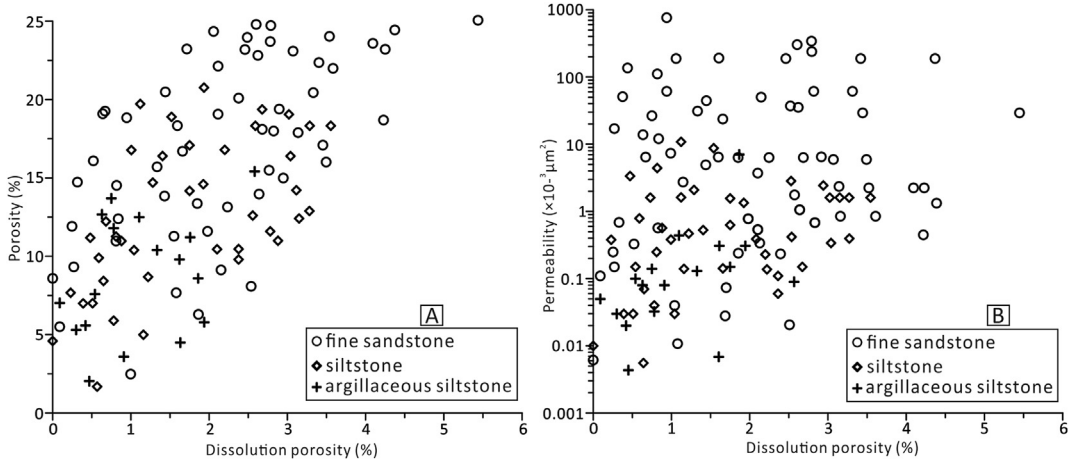

Fig. 13. Cross plots between (A) reservoir porosity and (B) reservoir permeability and dissolution porosity of the Eocene beach-bar sandstones in the Boxing Sag.

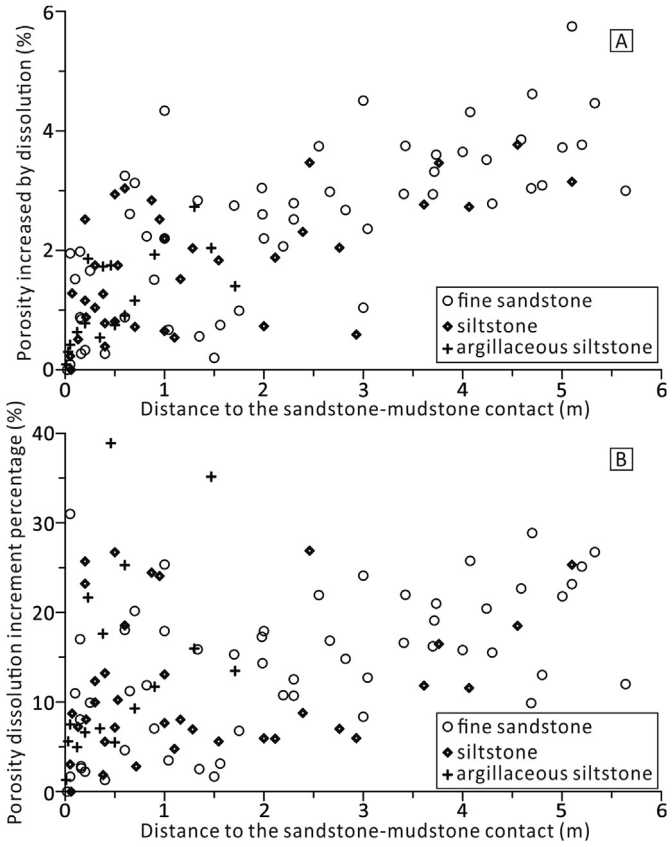

Fig. 14. Cross plots between (A) pore volume increased by dissolution and (B) the porosity dissolution increment percentage and distance to the mudstone-sandstone contacts of the Eocene beach-bar sandstones in the Boxing Sag.

Table 4
The classification standard of influence extent on reservoir quality of compaction, carbonate cementation and dissolution.

Intensity	$P_{compaction}$ (%)	$P_{cementation}$ (%)	$P_{dissolution}$ (%)
Strong	>70	>70	>70
Medium	70–30	70–30	70–30
Weak	30–0	30–0	30–0

medium compaction-weak feldspar dissolution-moderately carbonate cemented argillaceous siltstone facies (Type G). The reservoir properties of the seven types of sedimentary-diagenetic facies are summarized in Table 5.

The distribution of porosity and permeability of the seven sedimentary-diagenetic facies indicates that the variation ranges of porosity and permeability (log K) for a specific type of sedimentary-diagenetic facies are typically less than 6% and 1.2, respectively (Fig. 15). The influence of the sedimentary and diagenetic factors on the reservoir properties is generally in a relatively stable range for a specific sedimentary-diagenetic facies. However, the compaction degree typically increases with burial depths. Therefore, the trend lines of porosity and permeability for these sedimentary-diagenetic facies decrease gradually with depths. The trend lines of porosity can be described by power functions, with porosity as a dependent variable and depth as an independent variable, whereas the trend lines of log K can be best described by natural logarithm functions, with log K as a dependent variable and depth as an independent variable (Fig. 15). Using these distribution trend lines of porosity and log K of the sedimentary-diagenetic facies, the porosity and permeability (log K) of the Eocene beach-bar sandstone reservoirs can be prospected with an error of less than ±3% and ±0.6, respectively.

5.2. Log identification of sedimentary-diagenetic facies

Due to the limitation of the available core data in the study area, the identification of sedimentary-diagenetic facies of the Eocene beach-bar sandstone reservoirs from cores is quite limited. This hinders the reservoir prediction spatially. Wireline log data have been extensively applied to study high resolution sequence stratigraphy and sedimentary facies owing to their high vertical resolution and good continuity (Selley, 1992; Ozkan et al., 2011). Wireline logs such as acoustic travel time log (AC), compensated neutron log (CNL), compensated density log (DEN), resistivity log (RT) and the natural gamma ray log (GR) are closely related to the variations of rock and fluid properties, and are often used to identify rock types and properties. Log data can thus be used to identify sedimentary-diagenetic facies.

Conventionally rock properties was evaluated either using a single type of logs or composite logs, which usually results in relatively high uncertainties and/or non-unique interpretations (Selley, 1992; Ozkan et al., 2011). To improve log data interpretation and accuracy in the sedimentary-diagenetic facies identification, we used the Bayes discriminant analysis approach to classify the sedimentary-diagenetic facies from logs through evaluating and calibrating a suite of wireline log data (AC, CNL, DEN, RT, and GR) using core and petrographic data to build up a database for the seven sedimentary-diagenetic facies and the mudstone lithofacies. Systematic errors of wireline log data can be caused through the use of different types of logging instruments at different times. Therefore the logging data need to be standardized to eliminate these systematic errors. The rock properties of the thick mudstones (>5 m) are relatively stable and the corresponding logging data can be used as the basis for the standardization. Single wireline log (AC, CNL, DEN, RT, and GR) peaks of thick mudstones can be used as reference values in standardizing the wireline log data of the seven sedimentary-diagenetic facies (Fig. 16). The peak values of the AC, CNL, DEN, RT, and GR log data are 105 μs/ft, 33%, 2.05 g/cm^3, 87.5 API, and 3 Ω m, respectively (Fig. 16).

Table 5
Reservoir properties of the seven types of sedimentary-diagenetic facies of the Eocene beach-bar sandstone.

Sedimentary-diagenetic facies	Reservoir space	Porosity (%)	Permeability (mD)
Type A	Intergranular pores and dissolution pores	(12.2–25)/18.6	(0.4–767)/67.5
Type B	Mainly intergranular pores and minor dissolution pores	(5.2–17.1)/10.7	(0.08–11.1)/1.32
Type C	Mainly intergranular pores and minor dissolution pores	(7.7–18.9)/12.5	(0.04–10.6)/1.05
Type D	Mainly intergranular pores and minor dissolution pores	(5.0–11.8)/7.8	(0.04–5)/0.18
Type E	A small amount of intergranuler pores	(2.5–12.5)/6.7	(0.006–3.5)/0.19
Type F	A small amount of intergranuler pores	(1.7–7.0)/4.8	(0.002–0.15)/0.006
Type G	A small amount of micropores	(2.2–15.2)/6.8	(0.007–7.2)/0.13

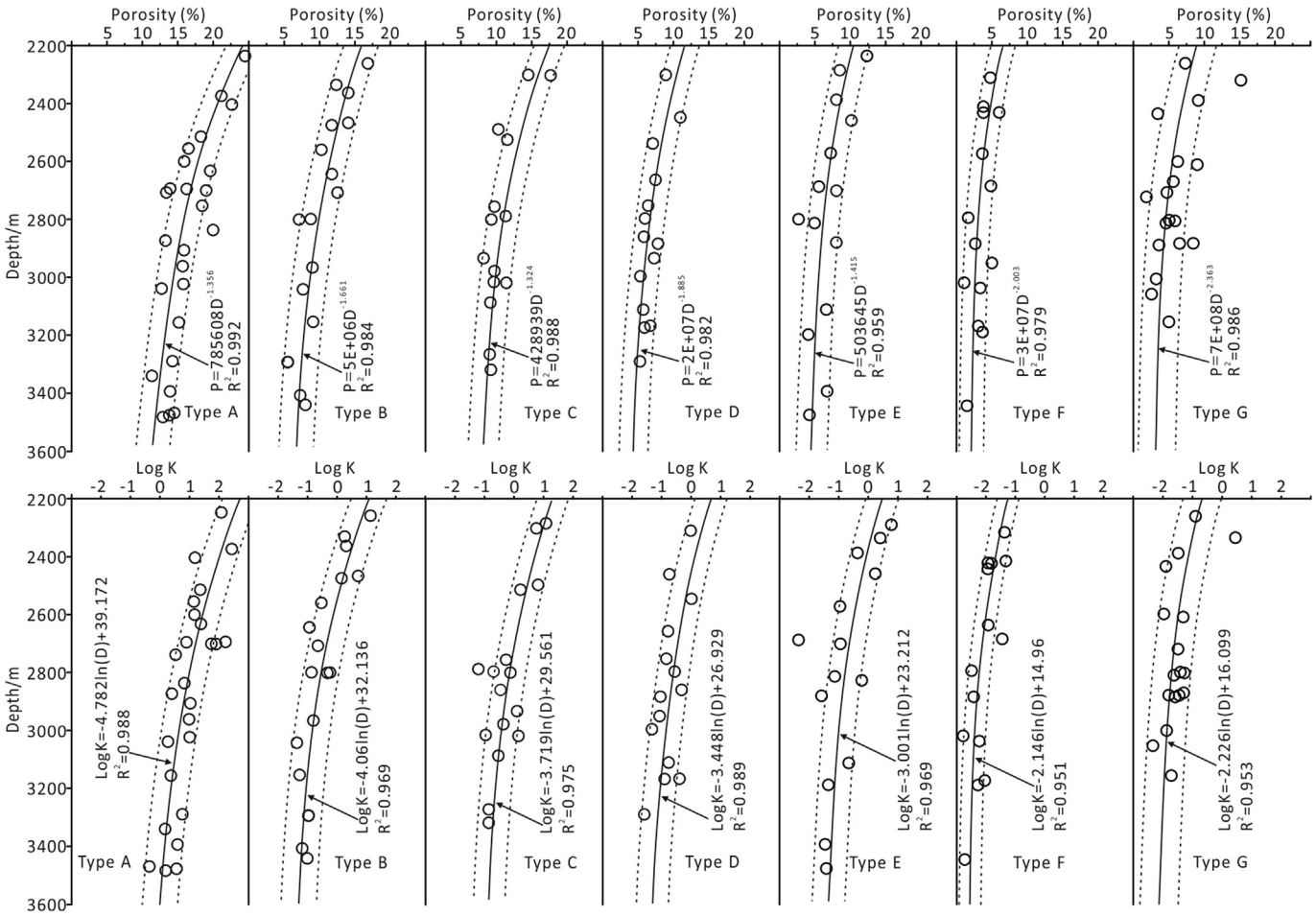

Fig. 15. Distribution and trend lines of porosity and permeability (log K) of the seven types of sedimentary-diagenetic facies of the Eocene beach-bar sandstone reservoirs.

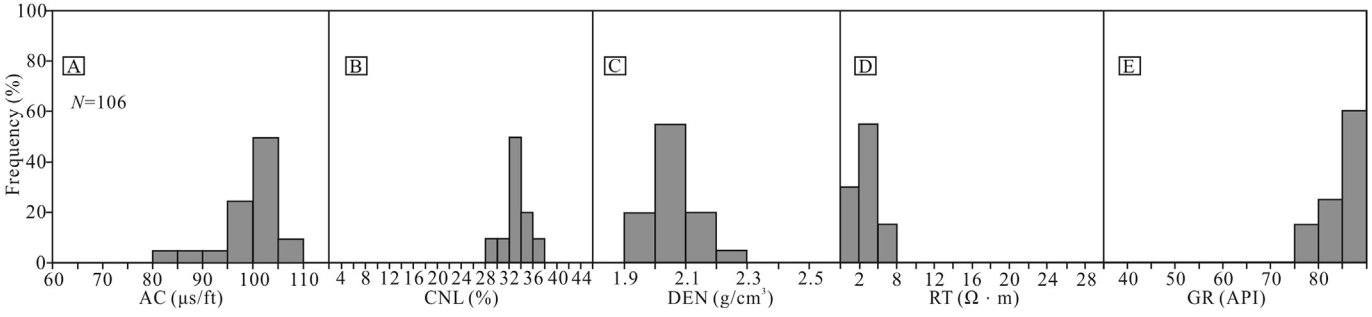

Fig. 16. Distribution of logging data of AC, CNL, DEN, RT, and GR of mudstones corresponding to the beach-bar sandstones in the Boxing Sag.

Fig. 17 shows the correlations of log data of GR-RT, GR-DEN, and AC-CNL of the seven sedimentary-diagenetic facies after the standardization. There is considerable variations in the ranges of the same wireline log data for different types of sedimentary-diagenetic facies (Fig. 17), which provides the basis for the Bayes discriminant analysis. The Bayes discriminant functions of the seven sedimentary-diagenetic facies were obtained using the SPSS software and based on the logging data:

Type A: $Y1 = 3.616AC - 1.508CNL + 512.767DEN + 0.689GR + 1.820R25 - 702.934$

Type B: $Y2 = 3.965AC - 1.249CNL + 585.075DEN + 0.792GR + 2.149R25 - 908.877$

Type C: $Y3 = 3.766AC - 1.795CNL + 590.661DEN + 0.673GR + 2.372R25 - 895.601$

Type D: $Y4 = 3.644AC - 2.182CNL + 579.421DEN + 1.099GR + 1.667R25 - 873.091$

Type E: $Y5 = 3.774AC - 1.252CNL + 540.225DEN + 0.958GR + 1.497R25 - 791.034$

Type F: $Y6 = 3.660AC - 1.232CNL + 563.948DEN + 1.266GR + 1.215R25 - 855.611$

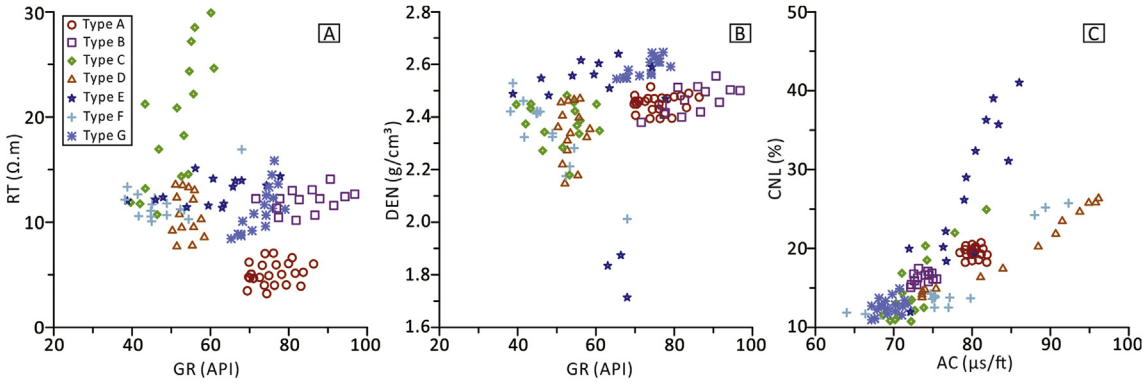

Fig. 17. Distribution of wireline log data of AC, CNL, DEN, RT, and GR of the seven sedimentary-diagenetic facies of the beach-bar sandstones in the Dongying depression.

Table 6
Discriminant probabilities of the seven types of sedimentary-diagenetic facies of the Eocene beach-bar sandstone reservoirs.

Types of S-D facies	Predicted Group membership							
	Type A	Type B	Type C	Type D	Type E	Type F	Type G	Total
Type A	66.1	0	33.9	0	0	0	0	100
Type B	0	100	0	0	0	0	0	100
Type C	0	0	93.5	0	6.5	0	0	100
Type D	0	0	0	100	0	0	0	100
Type E	0	0	0	0	100	0	0	100
Type F	0	0	0	0	0	100	0	100
Type G	0	0	31.4	0	0	0	68.6	100

Table 7
Verification of the accuracy of identification of sedimentary-diagenetic facies of the Eocene beach-bar sandstone reservoirs.

Well	Depth(m)	Y1	Y2	Y3	Y4	Y5	Y6	Y7	Bayes discriminant results	Cross plot results	Real type	R/W
F-1	3308.56	889.37	903.58	908.91	899.08	892.58	890.47	908.44	C	G	G	R
F-1	3308.81	885.99	899.60	904.70	894.58	888.74	885.97	904.59	C	G	G	R
F-1	3312.06	928.48	949.34	955.74	940.06	930.51	927.56	965.14	G	G	G	R
F-1	3309.56	896.29	911.29	917.40	905.54	898.06	894.70	920.48	G	G	G	R
F-1	3309.81	899.53	915.27	922.51	907.34	899.61	894.69	928.40	G	G	G	R
F-1	3317.94	911.39	927.86	932.52	921.88	915.59	913.10	931.77	C	G	G	R
F-1	3318.69	867.74	878.70	884.62	873.87	868.90	864.88	883.70	C	G	C	W
F-1	3318.44	858.12	866.61	870.98	861.53	859.07	853.70	868.41	C	C	C	R
F-1	3322.06	848.42	854.44	855.45	861.76	856.14	859.08	844.61	D	–	D	R
F-120	3323.06	852.59	857.77	862.59	868.45	858.09	860.46	853.13	D	–	D	R
F-129	3154.44	839.96	847.89	843.69	849.10	851.31	855.35	829.08	F	–	F	R
F-129	3154.69	838.25	845.61	841.67	847.33	849.24	853.06	827.14	F	–	F	R
F-129	3154.94	828.88	834.86	830.81	837.27	839.52	843.23	815.98	F	–	F	R
F-129	3155.69	742.18	736.48	731.58	737.41	747.33	745.87	715.18	E	–	E	R
F-129	3156.07	749.32	744.50	740.08	744.90	754.19	752.39	724.63	E	–	E	R
F-137	3170.40	783.20	780.62	776.88	775.85	786.48	780.12	762.11	E	–	E	R
F-137	3171.20	803.22	803.36	800.70	798.86	806.57	800.84	788.82	E	–	E	R
F-137	3171.40	812.03	813.73	810.44	809.78	816.89	812.66	798.20	E	–	E	R
F-137	3171.60	817.83	820.56	816.45	817.02	824.09	821.08	803.42	E	–	E	R
F-151	2728.48	778.52	777.17	780.33	777.58	778.90	775.00	771.21	C	A	A	R
G-351	2445.63	610.34	580.60	579.73	579.97	598.80	580.58	564.90	A	C	C	R
G-351	2445.88	657.78	636.24	631.63	632.55	652.38	638.14	615.15	A	A	A	R

Note: Y1–Y7 represents the calculation results of the seven Bayes discriminant functions using AC, CNL, DEN, RT, and GR log data. R-right; W-wrong.

$$\text{Type G: } Y7 = 3.785AC - 1.866CNL + 608.092DEN + 0.507GR + 3.189R25 - 944.583$$

The sedimentary-diagenetic facies of the Eocene beach-bar sandstones can be identified based on the principle of the maximum posterior probability of the Bayes discriminant analysis. The discriminant accuracy of all the seven types of sedimentary-diagenetic facies is presented in Table 6. The probability of discriminating the Type A sedimentary-diagenetic facies as Type A or Type C is 66.1% and 33.9%, respectively. The probability of discriminating the Type G sedimentary-diagenetic facies as Type G or Type C is 68.6% and 31.4%, respectively. The discriminant accuracies of the other types of sedimentary-diagenetic facies are greater than 93%. Cross-plots were used to distinguish Type A, C and G sedimentary-diagenetic facies, which have relatively low discriminant accuracies. The GR-RT and GR-DEN cross-plots indicate that the Type A, C and G sedimentary-diagenetic facies can be distinguished accurately with respect to the other sedimentary-

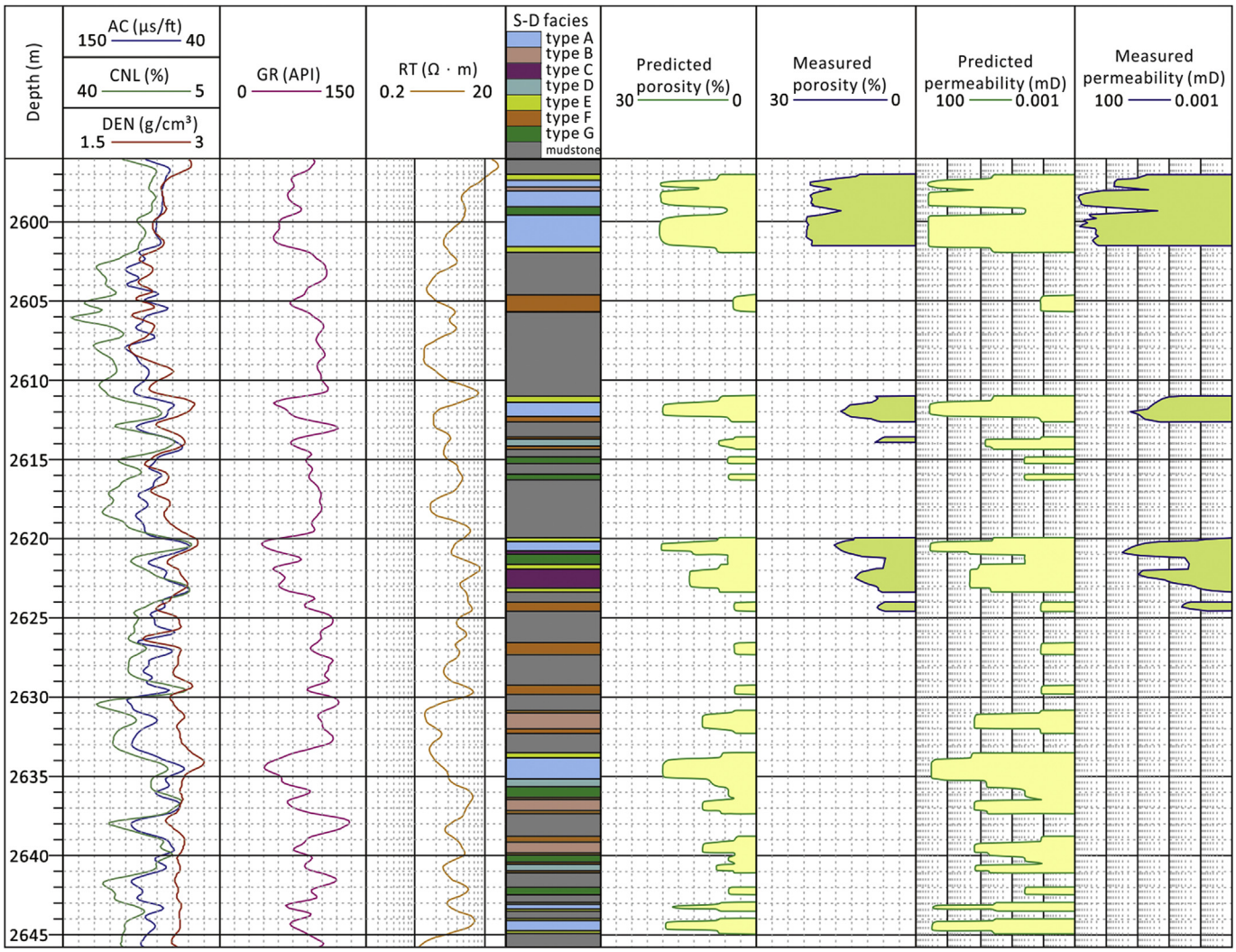

Fig. 18. Identification of sedimentary-diagenetic facies and prediction of porosity and permeability of the Eocene beach-bar sandstone reservoirs of the Well G-890.

diagenetic facies (Fig. 17A and B). The discriminant results of the Type A, C and G sedimentary-diagenetic facies are subject to the cross-correlations. The accuracy is 95.3%, based on back evaluation of the database through the Bayes discriminant functions and the cross-plots. The accuracy is up to 95.5% through verification of the other twenty-two datasets without the determination of the Bayes discriminant functions (Table 7). Therefore, the sedimentary-diagenetic facies can be identified effectively by using wireline log data through the use of Bayes discriminant analysis and corresponding cross-plots.

5.3. Prediction of reservoir porosity and permeability

The sedimentary-diagenetic facies of the Eocene beach-bar sandstone reservoir observed within the depth range of 2596–2646 m in Well G-890 was identified based on the aforementioned method (Fig. 18). All seven types of sedimentary-diagenetic facies were identified in the evaluated depth range of the well. Type A, B, C and D sedimentary-diagenetic facies are observed primarily in the centre of the thick fine sandstones and siltstones, and the Type E and F sedimentary-diagenetic facies are mainly distributed near the boundaries of thick sandstones and siltstones and in the thin fine sandstones and siltstones (Fig. 18). The diagenesis of interbedded mudstones caused the carbonate cement to precipitate primarily along the boundary area of the thick fine sandstones and siltstones (Li et al., 2014; Wang et al., 2016), which results in the development of a sedimentary-diagenetic facies with weak carbonate cementation in the centre of the thick sandstones and siltstones. A beach-bar deposit consists typically of several parasequences with upward increasing grain-size (Jiang et al., 2011), with lithologies usually changing from mudstone, argillaceous siltstone, siltstone and fine sandstone from the bottom to the top of the parasequences. The Type A, B and C sedimentary-diagenetic facies mainly develop at the top portion of the parasequences, while the Type D, E, F, and G sedimentary-diagenetic facies are mainly developed at the bottom portion of the parasequences (Fig. 18).

The porosities and permeabilities of the evaluated well (G-890) were predicted based on the distribution and the fitting equations of the trend lines derived for the seven sedimentary-diagenetic facies (Fig. 13). The predicted porosities and permeabilities of different sedimentary-diagenetic facies match the measured porosities and permeabilities well. The differences between the predicted and measured porosities and log K are generally in the range

of ±3% and ±0.6, indicating that the porosities predicted through the use of the sedimentary-diagenetic facies are reliable for reservoirs.

The porosity and permeability of the Type A sedimentary-diagenetic facies is higher than that of the Type B and C sedimentary-diagenetic facies. The Type D, E, F and G sedimentary-diagenetic facies have relatively low porosities and permeabilities. The sedimentary-diagenetic facies clearly control the distribution of porosities and permeabilities of reservoirs in Eocene beach-bar sandstones. Identification of sedimentary-diagenetic facies and prediction of their corresponding porosities and permeabilities thus provide an effective method to study and predict the favorable reservoirs for petroleum exploration and development in the study area.

6. Conclusions

A new reservoir porosity and permeability prediction method is presented. The method is primarily based on the identification of sedimentary-diagenetic facies, which are empirically and statistically correlated with porosity and permeability derived from cores and well log data. The workflow of the method is as the following: First, the types of sedimentary-diagenetic facies of the target reservoir are established based on detailed analysis of the sandstone litho-types and diagenesis. Second, the types and the trend lines of porosity and permeability for the sedimentary-diagenetic facies can be determined by the analysis of cores and corresponding data. Third, due to the high continuity and resolution of log data, the distribution of sedimentary-diagenetic facies within the study area is easily obtained based on the thin section and the Bayes discriminant analyses. Finally, the porosity and permeability of the reservoirs can be predicted relatively accurately without invoking core data.

The method was applied to predict the reservoir porosity and permeability of the Eocene beach-bar sandstones in the Dongying Depression, Bohai Bay Basin, in which seven sedimentary-diagenetic facies were identified. The variation ranges of porosity and permeability (log K) of the seven sedimentary-diagenetic facies are typically less than 6% and 1.2, respectively. The trend lines of porosity and log K have functional relationship with depth. The sedimentary-diagenetic facies can be identified effectively using log data through the use of the Bayes discriminant analysis and corresponding cross-plots. The porosity and permeability were predicted with errors in the range of ±3% and ±0.6, respectively, based on the distribution and the fitting equations of the trend lines for the seven types of sedimentary-diagenetic facies. The predicted porosity and permeability of the seven sedimentary-diagenetic facies match the measured porosities and permeability well.

The porosity and permeability prediction method described in this paper can be easily applied in the exploration and development of clastic reservoirs elsewhere.

Acknowledgments

This research work was jointly funded by the National Nature Science Foundation of China (Grant No. 41402095; Grant No. U1262203), the Chinese Postdoctoral Science Foundation (Grant No. 2014M550380; Grant No.2015T80760), and the Fundamental Research Funds for the Central Universities (16CX02027A), and the Scientific and Technological Innovation Project Financially Supported by the Qingdao National Laboratory for Marine Science and Technology (No. 2015ASKJ01). Thanks are also due to the Geosciences Institute of the Shengli Oilfield, SINOPEC, for permission to access their in-house database, providing background geologic data and permission to publish the results. Thanks are also due to Dr. Sven Egenhoff, Colorado State University, and anonymous reviewers for their constructive suggestions.

References

Ajdukiewicz, J.M., Lander, R.H., 2010. Sandstone reservoir quality prediction: the state of the art. AAPG Bull. 94, 1083–1091.
Ajdukiewicz, J.M., Nicholson, P.H., Esch, W.L., 2010. Prediction of deep reservoir quality using early diagenetic process models in the Jurassic Norphlet Formation, Gulf of Mexico. AAPG Bull. 94, 1189–1227.
Al-Ramadan, K., Morad, S., Proust, J.N., Al-Aasm, I.S., 2005. Distribution of diagenetic alterations in siliciclastic shoreface deposits within a sequence stratigraphic framework: evidence from the Upper Jurassic, Boulonnais, NW France. J. Sediment. Res. 75, 943–959.
Beard, D.C., Weyl, P.K., 1973. Influence of texture on porosity and permeability of unconsolidated sand. AAPG Bull. 57, 349–369.
Bjørkum, P.A., Oelkers, E.H., Nadeau, P.H., Walderhaug, O., Murphy, W.M., 1998. Porosity prediction in quartzose sandstones as a function of time, temperature, depth, stylolite frequency and hydrocarbon saturation. AAPG Bull. 82, 637–648.
Bloch, S., 1991. Empirical prediction of porosity and permeability in sandstones. AAPG Bull. 75, 1145–1160.
Bloch, S., Lander, R.H., Bonnell, L., 2002. Anomalously high porosity and permeability in deeply buried sandstone reservoirs: origin and predictability. AAPG Bull. 86, 301–328.
Boles, J.R., Franks, S.G., 1979. Clay diagenesis in Wilcox sandstones of southwest Texas: implications of smectite diagenesis on sandstone cementation. J. Sediment. Petrol. 49, 55–70.
Budd, D.A., 2002. The relative roles of compaction and early cementation in the destruction of permeability in carbonate grainstones: a case study from the Paleogene of west-central Florida, USA. J. Sediment. Res. 72, 116–128.
Carvalho, M.V.F., De Ros, L.F., Gomes, N.S., 1995. Carbonate cementation patterns and diagenetic reservoir facies in the Campos Basin Cretaceous turbidites, offshore eastern Brazil. Mar. Petrol. Geol. 12, 741–758.
Chen, D., Pang, X., Jiang, Z., Zeng, J., Qiu, N., Li, M., 2009. Reservoir characteristics and their effects on hydrocarbon accumulation in lacustrine turbidites in the Jiyang Super-depression, Bohai Bay Basin, China. Mar. Petrol. Geol. 26, 149–162.
De Souza, R.S., McBride, E.F., 2000. Diagenetic modeling and reservoir quality assessment and prediction: an integrated approach (abs.). AAPG Bull. 84, 1495.
Dutton, S.P., 2008. Calcite cement in Permian deep-water sandstones, Delaware Basin west Texas: origin, distribution, and effect on reservoir properties. AAPG Bull. 92, 765–787.
Dutton, S.P., Diggs, T.N., 1992. Evolution of porosity and permeability in the lower cretaceous travis peak formation, east Texas. AAPG Bull. 76, 252–269.
Ehrenberg, S.N., Nadeau, P.H., Steen, O., 2008. A megascale view of reservoir quality in producing sandstones from the offshore Gulf of Mexico. AAPG Bull. 92, 145–164.
Folk, R.L., 1974. Perology of Sedimentary Rock. Hemphill Publishing Co, Texas.
Folk, R.L., 1980. Petrology of Sedimentary Rocks. Hemphill Publishing, Austin, Texas, p. 182.
Friedman, G.M., 1958. Determination of sieve-size distribution from thin-section data for sedimentary petrological studies. J. Geol. 66, 384–416.
Friedman, G.M., 1962. Comparism of moment measures for sieving and thin-section data in sedimentary petrological studies. J. Sediment. Petrol. 32, 15–25.
Guo, S., Tan, L., Lin, C., Li, H., Lu, X., Wang, H., 2014. Hydrocarbon accumulation characteristics of beach-bar sandstones in the southern slope of the dongying sag, Jiyang depression, Bohai Bay Basin, China. Petrol. Sci. 11, 220–233.
Jiang, Z., Liu, H., Zhang, S., Su, X., Jiang, Z., 2011. Sedimentary characteristics of large-scale lacustrine beach-bars and their formation in the Eocene boxing sag of Bohai Bay Basin, east China. Sedimentology 58, 1087–1112.
Ketzer, J.M., Holz, M., Morad, S., Al-Aasm, I.S., 2003. Sequence stratigraphic distribution of diagenetic alterations in coal-bearing, paralic sandstones: evidence from the Rio Bonito Formation (early Permian), southern Brazil. Sedimentology 50, 855–877.
Lampe, C., Song, G., Cong, L., Mu, X., 2012. Fault control on hydrocarbon migration and accumulation in the Tertiary Dongying depression, Bohai Basin, China. AAPG Bull. 96, 983–1000.
Lander, R.H., Walderhaug, O., 1999. Porosity prediction through simulation of sandstone compaction and quartz cementation. AAPG Bull. 83, 433–449.
Li, Q., Jiang, Z., Liu, K., Zhang, C., You, X., 2014. Factors controlling reservoir properties and hydrocarbon accumulation of lacustrine deep-water turbidites in the Huimin Depression, Bohai Bay Basin, east China. Mar. Petrol. Geol. 57, 327–344.
Liu, H., Zhao, Y., Luo, Y., Chen, Z., He, S., 2015. Diagenetic facies controls on pore structure and rock electrical parameters in tight gas sandstone. J. Geophys. Eng. 12, 587–600.
Macaulay, C.I., Haszeldine, R.S., Fallick, A.E., 1993. Distribution, chemistry, isotopic composition and origin of diagenetic carbonates: magnus Sandstone, North Sea. J. Sediment. Res. 63, 33–43.
Marchand, A.M.E., Smalley, P.C., Haszeldine, R.S., Fallick, A.E., 2002. Note on the importance of hydrocarbon fill for reservoir quality prediction in sandstones. AAPG Bull. 86, 1561–1571.
McHargue, T.R., Price, R.C., 1982. Dolomite from clay in argillaceous limestones or shale associated marine carbonates. J. Sediment. Petrol. 52, 873–886.
McKinley, J.M., Atkinson, P.M., Lloyd, C.D., Ruffell, A.H., Worden, R.H., 2011. How

porosity and permeability vary spatially with grain size, sorting, cement volume, and mineral dissolution in fluvial triassic sandstones: the value of geostatistics and local regression. J. Sediment. Res. 81, 844–858.
Milliken, K.L., Land, L.S., 1993. The origin and fate of silt sized carbonate in subsurface Miocenee Oligocene mudstones, south Texas Gulf Coast. Sedimentology 40, 107–124.
Morad, S., Al-Ramadan, K., Ketzer, M., De Ros, L.F., 2010. The impact of diagenesis on the heterogeneity of sandstone reservoirs: a review of the role of depositional facies and sequence stratigraphy. AAPG Bull. 94, 1267–1309.
Morad, S., Ketzer, J.M., De Ros, L.F., 2000. Spatial and temporal distribution of diagenetic alterations in siliciclastic rocks: implications for mass transfer in sedimentary basins. Sedimentology 47, 95–120.
Mou, D.C., Brenner, R.L., 1982. Control of reservoir properties of tensleep sandstone by depositional and diagenetic facies; lost soldier field. Wyo. J. Sediment. Res. 52, 367–381.
Okoro, A.U., Igwe, E.O., 2014. Lithofacies and depositional environment of the amasiri sandstone, southern benue trough, Nigeria. J. Afr. Earth Sci. 100, 179–190.
Ozkan, A., Cumella, S.P., Milliken, K.L., Laubach, S.E., 2011. Prediction of lithofacies and reservoir quality using well logs, late cretaceous williams fork formation, mamm creek field, Piceance basin, Colorado. AAPG Bull. 95, 1699–1723.
Paxton, S.T., Szabo, J.O., Ajdukiewicz, J.M., Klimentidis, R.E., 2002. Construction of an intergranular volume compaction curve for evaluating and predicting compaction and porosity loss in rigid-grain sandstone reservoirs. AAPG Bull. 86, 2047–2067.
Rossi, C., Marfil, R., Ramseyer, K., Permanyer, A., 2001. Facies-related diagenesis and multiphase siderite cementation and dissolution in the reservoir sandstones of the Khatatba Formation, Egypt's Western Desert. J. Sediment. Res. 71, 459–472.
Salem, A.M., Ketzer, J.M., Morad, S., Rizk, R.R., Al-Aasm, I.S., 2005. Diagenesis and reservoir-quality evolution of incised-valley sandstones: evidence from the abu madi gas reservoirs (upper miocene), the nile delta basin, Egypt. J. Sediment. Res. 75, 572–584.
Schmoker, J.W., Gautier, D.L., 1988. Sandstone porosity as a function of thermal maturity. Geology 16, 1007–1010.
Schmoker, J.W., Schenk, C.J., 1994. Regional trends of the upper Jurassic Norphlet Formation in southwestern Alabama and vicinity, with comparisons to formations of other basins. AAPG Bull. 78, 166–180.
Selley, R.C., 1992. The third age of wireline log analysis: application to reservoir diagenesis. Geol. Soc. (Lon.) Spec. Publ. 65, 377–387.
Shinn, Y.J., Lee, H.S., Kwon, Y.K., Kwak, W.J., 2014. Lithofacies distribution and depositional environment in the Lower Cretaceous McMurray Formation, BlackGold Lease, northern Alberta: implications for geometry and distribution of oil sand reservoirs. Geosci. J. 18, 325–337.
Taylor, K.G., Gawthorpe, R.L., Curtis, C.D., Marshall, J.D., Awwiller, D.N., 2000. Carbonate cementation in a sequence-stratigraphic framework: upper cretaceous sandstones, book cliffs, Utah–Colorado. J. Sediment. Res. 70, 360–372.
Taylor, T.R., Giles, M.R., Hathon, L.A., Diggs, T.N., Braunsdorf, N.R., Birbiglia, G.V., 2010. Sandstone diagenesis and reservoir quality prediction: models, myths, and reality. AAPG Bull. 94, 1093–1132.
Tobin, R.C., McClain, T., Lieber, R.B., Ozkan, A., Banfield, L.A., Marchand, A.M.E., 2010. Reservoir quality modeling of tight gas sands in Wamsutter field: integration of diagenesis, petroleum systems and production data. AAPG Bull. 94, 1229–1266.
Udden, J.A., 1914. Mechanical composition of clastic sediments. GSA Bull. 25, 655–744.
Walderhaug, O., 2000. Modeling quartz cementation and porosity loss in middle jurassic brent group sandstones of the kvitebjørn field, northern north sea. AAPG Bull. 84, 1325–1339.
Wang, J., Cao, Y., Liu, K., Liu, J., Xue, X., Xu, Q., 2016. Pore fluid evolution, distribution and water-rock interactions of carbonate cements in red-bed sandstone reservoirs in the Dongying Depression, China. Mar. Petrol. Geol. 72, 279–294.
Wentworth, C.K., 1922. A scale of grade and class terms for clastic sediments. J. Geol. 30, 377–392.
Worden, R.H., Mayall, M., Evans, I.J., 2000. The effect of ductile-lithic sand grains and quartz cement on porosity and permeability in Oligocene and lower Miocene clastics, South China Sea: prediction of reservoir quality. AAPG Bull. 84, 345–359.